

SENSITIVITY ANALYSIS OF THE SPATIAL AND ALTITUDE DISTRIBUTIONS OF POLLUTANTS USING THE WEATHER RESEARCH AND FORECASTING MODEL WITH CHEMISTRY (WRF/CHEM)

Rafael P. Fernandez^{a,b}, Pablo G. Cremades^{a,b}, David G. Allende^{a,b} and S. Enrique Puliafito^{a,b}

^a*Grupo de Estudios Atmosféricos y Ambientales (GEAA), Universidad Tecnológica Nacional – Facultad Regional Mendoza. Rodríguez 273, 5500 Mendoza, Argentina.
<http://www.frm.utn.edu.ar/geaa/> — rpfernandez@uncu.edu.ar*

^b*Consejo Nacional de Investigaciones Científicas y Técnicas (CONICET)*

Keywords: Regional Air Quality, WRF/Chem, Altitude Emissions Distributions.

Abstract: The Weather Research and Forecasting (WRF) model is a new “state-of-the-art” meteorological model which offers the users many different options for physical parameterizations. The recent introduction of a Chemical module (WRF/Chem) allows to perform an “on-line” description of the chemical evolution of trace pollutants by coupling a time-dependent chemical mechanism to the primitive meteorological equations. The advantage of WRF/Chem model over traditional dispersion models (CALPUFF, ISC3, etc.) is that a 3-D+temporal description of the pollutants distribution can be obtained. In this work, the WRF/Chem model has been used to study the dependence of the spatial and temporal distribution of point sources of pollutants with the altitude at which they are emitted. The study considers a detailed 24 hours winter period over a 200 km × 200 km regional domain centered at Buenos Aires, including only the pollutants emissions from typical power-plant stack with variable height. A sensitivity analysis of the model was performed considering different scenarios where the altitude and emission rate of the stack were modified, keeping the total emission constant. The response of WRF/Chem model to the proposed cases was statistically analyzed by computing several types of difference measures, as mean bias error, mean absolute error and index of agreement. Larger sensitivity to emissions schemes was found for the scenarios emitting near surface or at elevated levels. For those emitting at intermediate levels, the height of the time-variant Planetary Boundary Layer (PBL) is a relevant parameter.

1 INTRODUCTION

Air quality prediction is a very complex topic that involves both meteorological factors (wind speed and direction, turbulence, radiation, precipitation, etc.) and chemical processes (emissions, deposition and chemical reactivity). Even though *Numerical Weather Prediction* models (NWP) have originally been developed to simulate only the meteorological component, in the real atmosphere physical and chemical processes are highly coupled and occur simultaneously (Grell et al. 2005). For example, chemistry affects meteorology throughout its direct effect on the radiative balance of the atmosphere, while clouds and precipitation directly modify the transformation and removal of pollutants.

In the last few years, the use of numerical *Chemical Transport Models* (CTM) has become an indispensable tool in order to study the effect of pollutants on the environment and/or the population health (Puliafito and Quaranta, 2009). CTMs usually couple the chemistry to the meteorology by solving a validated chemical mechanism into a 2-D or 3-D physical coordinate system, which in turn has been previously modeled with NWPs in order to obtain the pressure, temperature and wind speed/direction fields. Continuous advances in computing capacity have made possible to improve CTMs applications, increasing the size of spatial domains, increasing the grid step resolution and adapting the internal temporal steps. The correct implementation of CTMs allows users to identify the contribution of each independent source as well as to evaluate the impact of each pollutant on the air quality of the surrounding area.

The *Weather Research and Forecasting* model (WRF) is a novel meteorological model developed cooperatively by prestigious research centers (NCAR, NOAA, etc; Michalakes et al. 2002). Recently, a strong effort has been done to incorporate a chemical module to the WRF model with the purpose of simultaneously solving a reaction mechanism into a unique spatial-temporal coordinate system. The development of the new WRF/Chem model (*WRF with Chemistry*) constitutes an adaptable and useful tool intended to perform the "on-line" modeling of the chemistry and meteorology over a wide range of scales (Grell et al. 2005). The advantage of WRF/Chem over other traditional dispersion models such as CALPUFF (Scire et al. 2000) or ISC3 (US EPA, 1995) is that a 3-D+temporal description of the pollutants distribution can be obtained, including the continuous coupling between chemistry and meteorology.

The WRF/Chem model has been used to determine the ozone concentration in topographical complex regions (Schürmann et al. 2009), to obtain the spatial-temporal variation of pollutants for different emissions scenarios (Ying et al. 2009), to estimate the transport and deposition of acid and toxic substances (Meiyun et al. 2008), among many other applications. Whenever experimental data was available, research works had compared the modeled results with observations, focusing the analysis on the surface distributions of pollutants and their temporal variation. Precise

results of a 3-D air quality model depends on an accurate spatial and temporal characterization of the pollutants emissions, i.e. altitude, temperature and emission rate of industrial sources (Placet et al. 2000; Seinfeld and Pandis, 2006).

However, neither vertical concentration profiles nor spatial distributions of pollutants concentration have been sufficiently described. In this work, we present a vertical sensitivity analysis of the WRF/Chem model. Even though results are general, this exercise requires a local configuration. Therefore, we setup the model to describe the air quality of Buenos Aires. While the WRF model includes a default global setup which can be used over any selected domain and in any part of the world, a correct regional configuration requires to include the local topography, the characteristics of soils and land use, and the magnitude and type of anthropogenic emissions.

For this analysis we designed 9 hypothetical emissions scenarios, considering 4 height-variant power-plants stacks with emissions rates similar to the ones located nearby urban centers. The ambient concentration and distributions of SO₂, CO and NO₂ is analyzed for the 4 lower atmospheric levels, quantifying differences observed when the different scenarios are considered. The statistical analysis was made according to Wilmott (1982).

2 MODEL DESCRIPTION

This section introduces a brief description of the WRF/Chem model. Then, the regional configuration of the model is described, addressing the changes performed to several modules in order to include the local characteristics of the studied region. A description of the studied area and model setup is given, showing the physical and chemical parameterizations used for this work. Finally, we describe the proposed scenarios with different stack emissions for Buenos Aires.

2.1 WRF/Chem Model

The mass-coordinate “non-hydrostatic” version of WRF (usually called *Advanced Research WRF* or ARW) possesses the most convenient features to perform the “on-line” modeling of the atmospheric chemistry (Wang et al. 2009). The model solves the physical primitive equations into a regional scale domain preserving scalar and mass fluxes from initial and boundary conditions obtained from global circulation models. It includes several dynamic cores and physical parameterizations to represent a wide and multiscale range of processes. The WRF/Chem model has a modular structure that allows the introduction of a variety of coupled physical-chemistry processes such as: emission, transport and deposition of pollutants, chemical transformation, aerosols direct and indirect effects, radiative transference, and photolytic processes. (Peckham et al. 2010). The Chem module relies on both, a proper local configuration and the inclusion of emissions inventories with high spatial and temporal resolution.

In order perform the proposed sensitivity analysis, the default physical and chemical parameterizations included in WRF/Chem model were used. Physical parameterizations include (Wang et al. 2009): a 5-class WSM microphysical model, a

Goddard radiative transfer scheme for shortwave radiation, a unified Noah model for surface physics, and the YSU (Monin-Obukhov) scheme to compute the Planetary Boundary Layer (PBL) evolution. The chemical parameterizations include the RADM2 mechanism (*Regional Acid Deposition Model, v. 2*; Stockwell et al. 1990), a photolysis rate constant computation using the Fast-J method, and a volumetric approximation of the aerosols optical properties (Peckham et al. 2010), among others.

2.2 Regional Configuration

Both WRF-ARW and WRF/Chem models must be locally configured to include the particular characteristic of the studied area. Because of their complexity, there is a default configuration that has been optimized for modeling any regional domain on the planet using static global data. However, for operative applications inside the United States, Europe and Asia, advanced configurations have been developed allowing the inclusion of high resolution spatial-temporal local input data (Schürmann et al. 2009; Zhang et al. 2010; among others). Accordingly, GEAA (*Grupo de Estudios Atmosféricos y Ambientales*) is working on the development of the most convenient local configurations to perform regional studies in Argentina.

The complex terrain geography of Argentina requires the inclusion of a correct topographic description of the region, using high resolution terrain elevation data. The WRF *Preprocessing System* (WPS) module configuration was modified to introduce the *Shuttle Radar Topography Mission* (SRTM3) data (Rodríguez et al. 2005), increasing terrain elevation resolution more than 10 times, with 3" × 3" (90 m × 90 m) satellite processed data.

Land Use Land Cover (LULC) data is another important static field to consider, because it strongly affects the surface heat transfer rates and the natural biogenic emissions. LULC maps developed by several national institutions and agencies (INTA, National Universities, etc.; Cruzate et al. 2007; Puliafito and Allende, 2007; Allende et al. 2010) have been adapted for several regions and are actually being implemented into the WPS module. A *Geographical Information System* (GIS) was used to classify the maps according to the 24 standard USGS classes (*United States Geological Survey*; Wang et al. 2009).

Before a chemical/meteorological modeling is performed, WRF/Chem must be set up with certain boundary and initial conditions in order to solve the primitive differential equations system. The meteorological FNL (*Final Analysis*) initial and boundary fields from the NCEP's *Global Forecast System* (GFS; RDA, 2010) were used for this study. In order to eliminate interferences with the results, no external background pollutant concentrations from global CTMs (such as the *Model for OZone And Related chemical Tracers*, MOZART; Emmons et al. 2010) were included, considering only the default WRF/Chem input options.

2.3 Regional Area Description

The modeled area used to perform the sensitive analysis consists of a 200 km ×

200 km square domain with a 4 km grid resolution centered at the city of Buenos Aires ($34^{\circ} 62' S$, $58^{\circ} 45' W$). Figure 1 shows a Conic Lambert-Conformal projection of the selected domain, as well as the terrain elevation. A complete period of 1 winter week (13–20 August, 2007) was initially analyzed in order to determine the existence of persistent meteorological conditions. The results presented in Section 4 correspond to the most representative day (August 14th, 2007), showing the hourly variations observed for the different scenarios for a 24 hours period.

A standard WRF/Chem set of 28 ETA vertical levels were used for all the calculations. As reference, the initial equivalent altitude and pressure for the 10 lower levels at the center point of domain for the initial time are presented in Table 1.

The altitude of stack emissions for the different scenarios was changed within the lower 4 ETA levels, including the surface (see Section 3). The reason for selecting a standard vertical ETA resolution was to ease the comparison of the present analysis with other studies over different regional domains and areas.

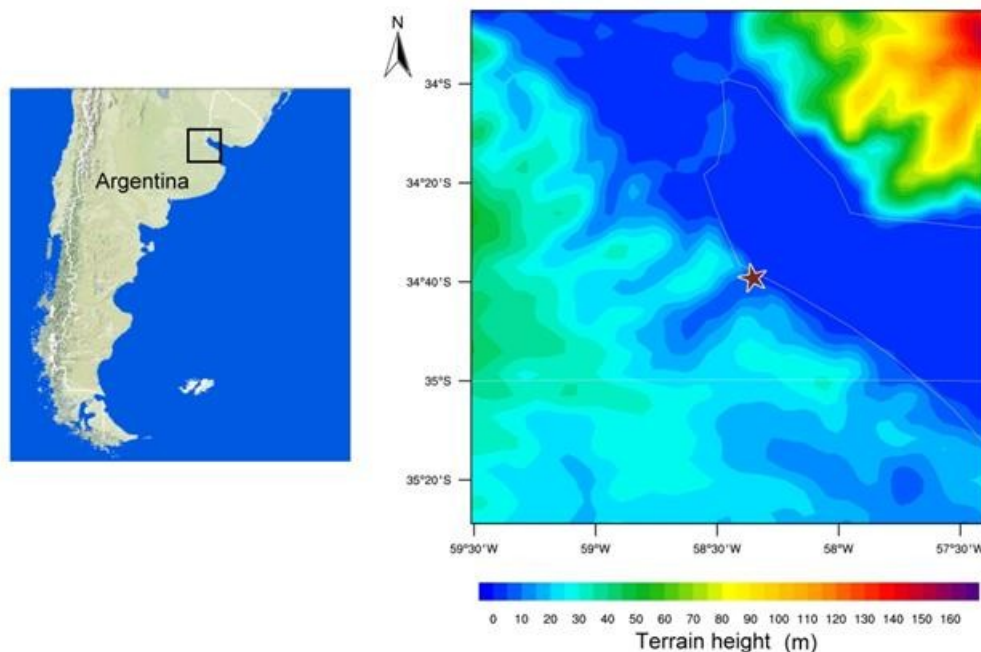


Figure 1: Modeling regional domain centered in the city of Buenos Aires (right). The terrain is mainly flat with small elevations up to 180 m, increasing to the SW and to the NE of the *Río de la Plata*. A 4 km grid resolution is considered adequate to capture the topography singularities and to keep computational resources reasonable. The star shows the location of the hypothetical power plant stack.

Level	η	Equivalent Altitude (m)	Pressure (hPa)
ETA_0	0.9965	28.3	1006.3
ETA_1	0.9880	97.8	998.1
ETA_2	0.9765	193.2	987.0
ETA_3	0.9620	315.2	973.0

<i>ETA_4</i>	0.9440	469.0	955.5
<i>ETA_5</i>	0.9215	665.0	933.8
<i>ETA_6</i>	0.8945	905.7	907.8
<i>ETA_7</i>	0.8548	1272.0	869.5
<i>ETA_8</i>	0.8044	1754.4	821.0
<i>ETA_9</i>	0.7539	2260.2	772.6
<i>ETA_10</i>	0.7035	2792.6	724.2

Table 1: Initial equivalent altitude (m) and pressure (Pa) of the 10 lower ETA vertical levels included in the model. The levels considered for the different scenarios are bold highlighted.

3 POLLUTANTS EMISSION

The inclusion of primary pollutants into air quality models is usually performed considering different types of emissions inventories: residential, mobile and industrial. While residential and vehicle emissions occur only at the surface level, as area-type emissions, industrial sources are usually well localized elevated point emission, which are described by emission rate, stack physical parameters (diameter and height), exit mass flux and temperature of the pollutant emitted.

GEAA has developed a detailed emission inventory for the city of Buenos Aires which includes the industrial emissions from the power-plants nearby the city and the industrial pole of Dock Sud (Allende et al. 2010). These sources are associated to more than 50 stack emissions, each one with its speciation, average rate and temporal variation. A representative point source with variable altitude was setup in the model. Its altitude varies between ETA level 0 and ETA level 3, which is the case of real industrial stacks in the area. The total emission rate for all scenarios was kept constant with the following values: [CO] = 3.07 g/s, [NO_x] = 54.61 g/s and [SO₂] = 61.18 g/s.

The inclusion of the pollutants emissions into WRF/Chem model was performed adapting the *emiss_v3* routine originally developed to process the United States *National Emissions Inventory* database (NEI, 2005), which generates chemical emissions input files (*wrfchemi*) over a standard lower atmosphere with 19 altitude levels. Emissions are interpolated on runtime and accommodated into the 4 lower ETA levels included into WRF/Chem.

3.1 Emissions Scenarios

Different emissions scenarios were proposed to analyze the response of WRF/Chem model to the vertical allocation of the emissions. The total emission of pollutants was kept constant for all scenarios, changing the height of emissions of 4 stacks (each one with 25 % of the total emission rate) so the emission occurs at the middle of each of the 4 lower levels named (from surface upwards): *ETA_0*, *ETA_1*, *ETA_2* and *ETA_3* (see Table 1). Table 2 presents the 9 emission scenarios selected for this study and shows the percentage of the total emission on each level.

Altitude	ETA_0	ETA_1	ETA_2	ETA_3
ALL_0	100%	—	—	—
ALL_1	—	100%	—	—
ALL_2	—	—	100%	—
ALL_3	—	—	—	100%
AVG	25%	25%	25%	25%
MID	—	50%	50%	—
EXT	50%	—	—	50%
WANG1	5%	30%	60%	5%
WANG2	5%	60%	30%	5%

Table 2: Description of the emissions scenarios considered for the sensitive analysis. The emissions percentages were obtained by changing the altitude of 4 stacks.

The *ALL_#* scenarios (*ALL_0*, *ALL_1*, *ALL_2* and *ALL_3*) are used for the study because they represent the most extreme differences of pollutants emissions, and the changes in ambient concentrations are easily observed. The selection of the *WANG1* and *WANG2* scenarios is based on Wang et al. 2010, where an altitude distribution of stack emissions for different industries and species is given.

4 RESULTS AND DISCUSION

In order to introduce non-atmospheric researchers to air quality studies, Sections 4.1 to 4.3 present a qualitative and graphical description of 3-D+temporal (surface, altitude, and temporal) ambient SO₂ concentration distributions obtained with WRF/Chem for the *ALL_#* scenarios. Then, in Section 4.4 a description of the absolute and relative differences in the ambient concentrations for the 4 lowers ETA levels is shown. Finally, a statistical and quantitative description of the main biases observed between all the presented scenarios is summarized in Section 4.5. When other emitted species such as CO and NO_x are considered, similar results are obtained.

4.1 Surface Distributions

Figure 2 shows the horizontal surface distributions of SO₂ concentrations at 12:00 GMT (*Greenwich Mean Time*) for the four ETA levels for the *ALL_0* scenario. The red line represents the main direction of the SO₂ plume following the horizontal wind field.

Ambient concentration is greater for *ETA_0* level (were the emission is taking place) and diminishes as the altitude increases. Also, the plume direction is different in all levels, reflecting the capability of WRF/Chem to simulate the wind field among atmospheric levels and to compute independently the horizontal transport at different altitudes. Note how the maximum concentration at each level is located farther from the source as the altitude increases. Moreover, the ambient concentration on each horizontal plane is more homogeneously distributed, as a

consequence of the increasing non-turbulent dispersion.

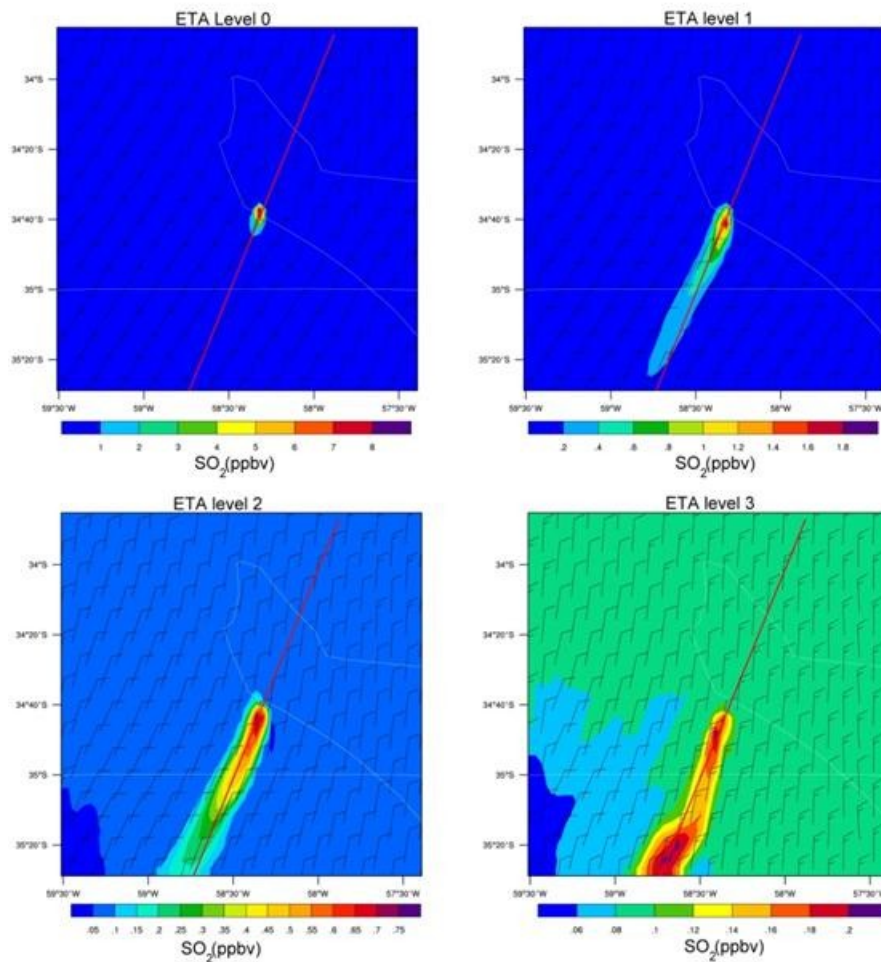


Figure 2: Surface distribution of SO_2 for the 4 lower ETA levels for the *ALL_0* scenario. Wind barbs show each level wind field, while the red line indicates the main direction of the plume trajectory. Note that the scale on each panel is different.

The ambient concentrations for the same levels but when the *ALL_3* scenario is considered is shown in Figure 3. The plume direction is quite different to the one observed in Figure 2, making evident that the wind speed and direction at the emission level are different than those at the surface. Also, the dispersion pattern for each level behaves differently to the one observed for the *ALL_0* scenario: the pollutant mixing is higher at the surface (*ETA_0*) while the maximum absolute values are observed at *ETA_3* level (where emission occurs). The high values at the domain border may be a consequence of an incorrect boundary condition description (such as neglecting the inclusion of MOZART data).

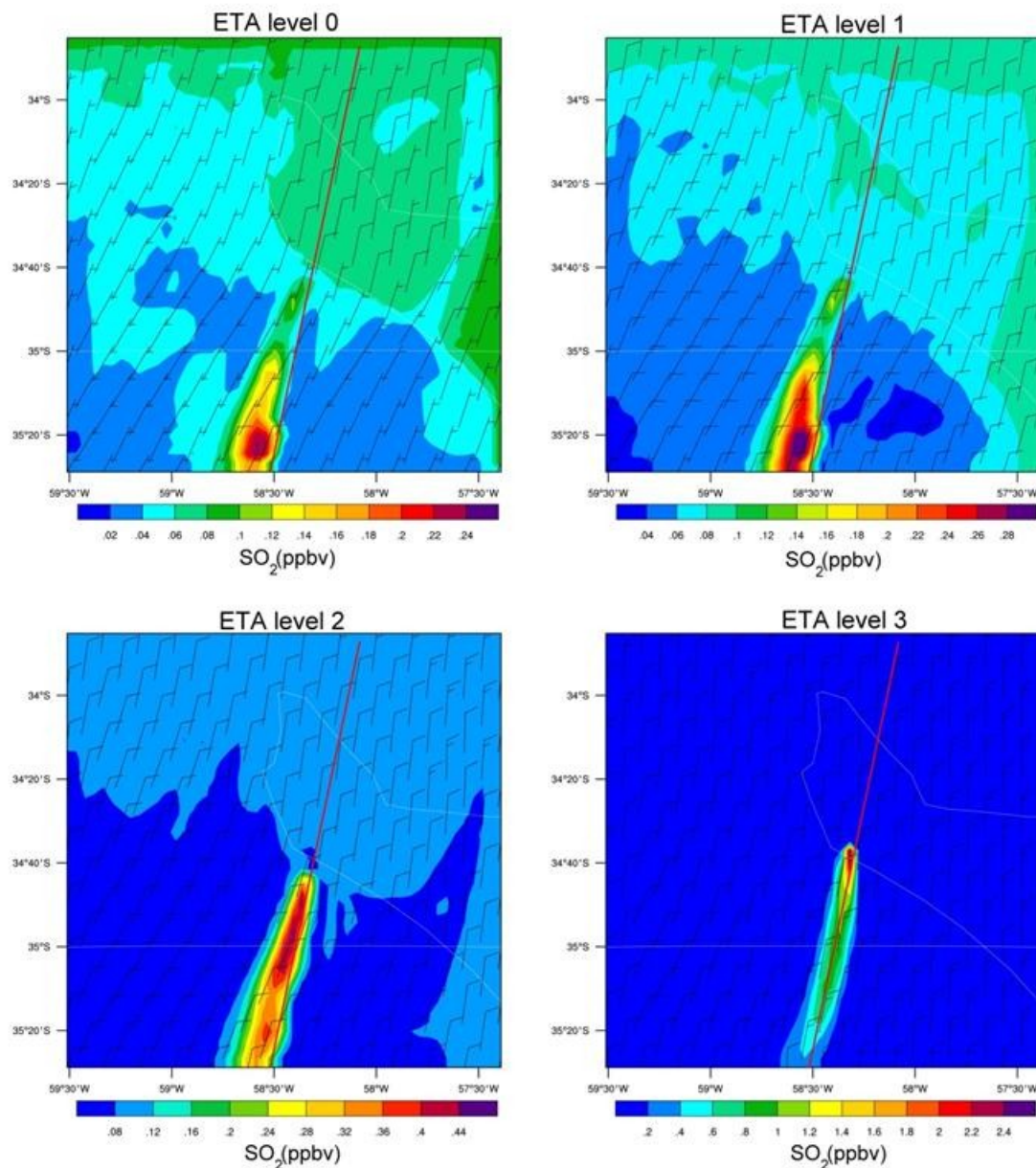


Figure 3: Idem Figure 2 but for the *ALL_3* scenario.

When the emission occurs at the surface (*ALL_0*), the *ETA_0* level concentration reaches 8 ppb and the *ETA_3* level maximum concentration is below 0.25 ppb. For the *ALL_3* case, the maximum concentration on the emitting level is 3-4 times smaller (below 2.5 ppb) while the concentration on the *ETA_0* level is similar to the *ALL_0* case (0.2 ppb). When the emissions take place at higher levels (e.g. *ALL_3*), the dispersion over each underlying level is greater than when emitting in the lowest level (e.g. *ALL_0*).

4.2 Altitude Distributions

Figure 4 shows the vertical profile of the SO₂ concentrations following the plume direction for the *ALL_#* scenarios. The peak concentration values occur at the level of

emission. When emission occurs in the three lower levels, the PBL height has not been surpassed, and concentrations are very high at the surface and near the source. For the *ALL_3* case, the PBL plays an important role in SO_2 dispersion, making surface concentration level lower and a pseudo-symmetrical profile in the vertical direction.

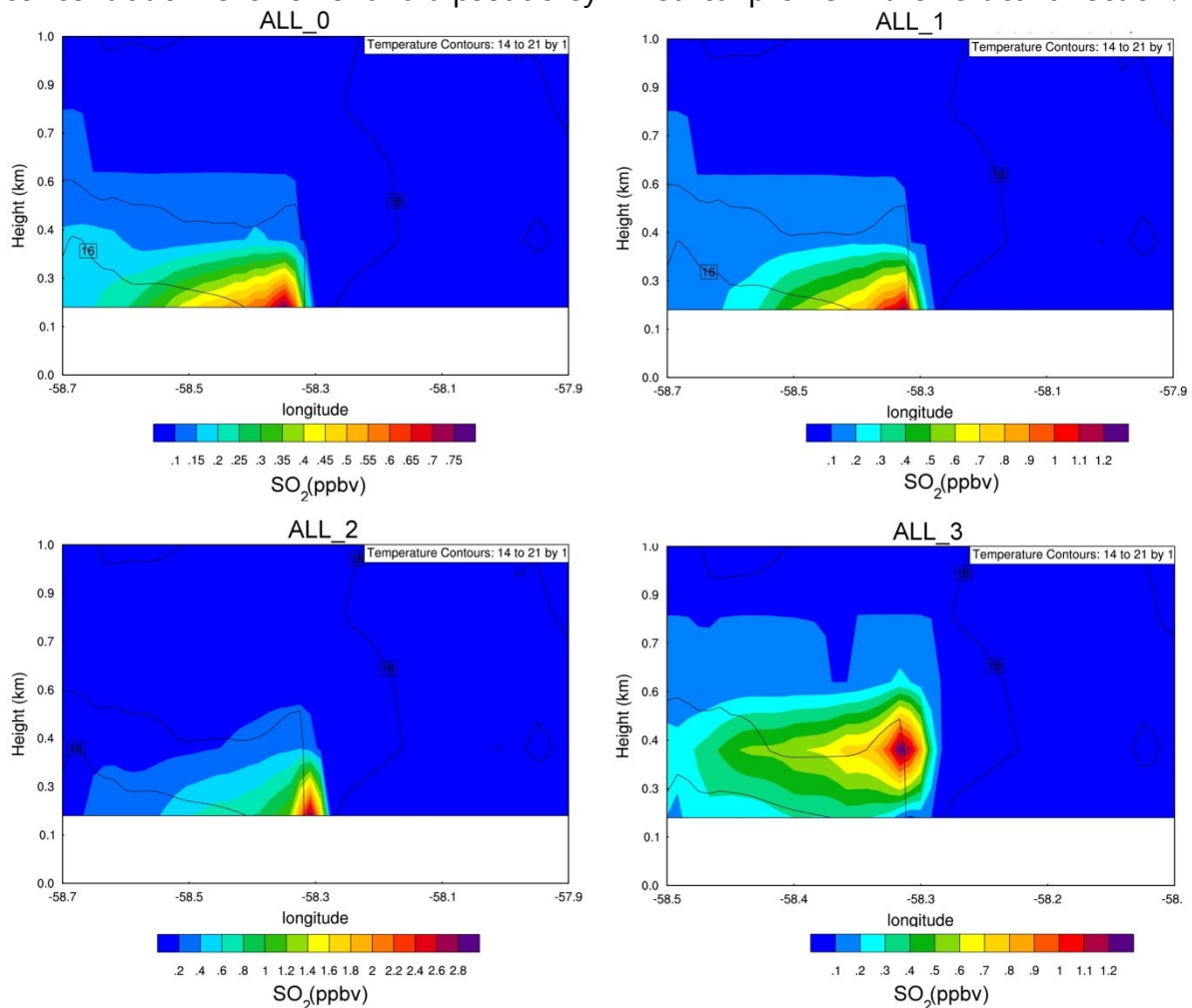


Figure 4: Altitude distribution of SO_2 for the *ALL_#* scenarios. The abscissas axes represent the longitude of the vertical plane selected. Note how as the altitude of emissions increases, the ambient concentration on the surface diminishes.

4.3 Temporal Variations

The temporal evolution of SO_2 concentration at *ETA_0* level, the top level (*ETA_3*) and vertical profile for the *ALL_0* scenario is shown in Figure 5. As the wind field changes from East (00:00) to North (18:00), the plume rotates continuously in a different way for each level. Consequently, area of impact will not be the same for the different emissions scenarios neither at surface nor at any vertical level.

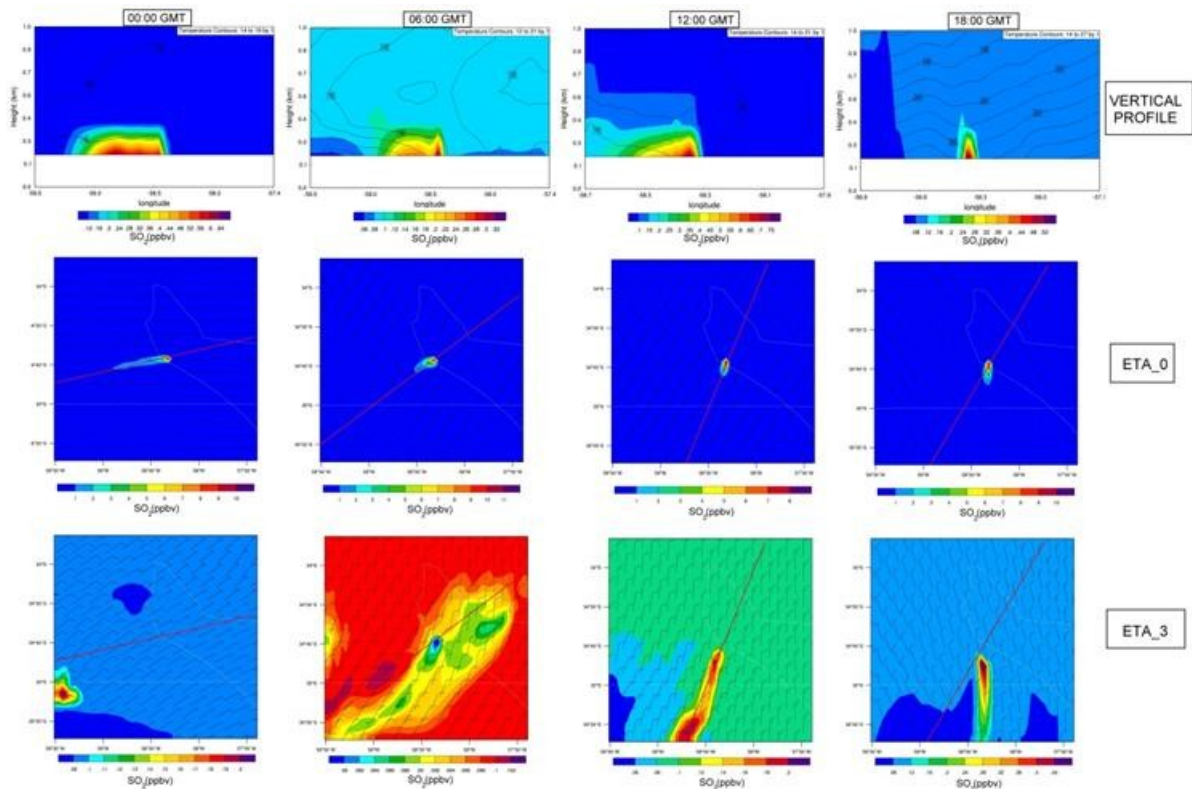


Figure 5: Temporal evolution of the SO₂ concentration between 00:00 and 18:00 GMT for the ALL_0 scenario.

The upper panel presents the vertical profiles, while the lower panels show the SO₂ concentrations contour plot at ETA_0 (middle) and ETA_3 (bottom) levels.

A similar behavior as the one observed on Figure 5 can be found for each one of the ALL_# scenarios. As an example, Figure 6 shows the time dependent vertical, ETA_0 and ETA_3 levels concentrations for the ALL_3 scenario. Even though the temporal evolution follows the same patterns, the absolute SO₂ concentration above every grid-point changes from level to level and from scenario to scenario. The following section shows the differences found on the ambient concentrations of each level for the different scenarios.

4.4 Differences Between Scenarios

Once the main characteristics of the case of study have been presented, a quantitative estimation of the differences observed between different scenarios is given. We show the absolute and relative differences on the ambient concentrations when different scenarios are considered. All the scenarios have been compared by pairs, and the following variables have been calculated according to Eq. (1) and Eq. (2):

$$Diff_{i-j}^{\#} = Conc_i^{\#} - Conc_j^{\#} \quad (1)$$

$$Rel_{i-j}^{\#} = \frac{(Conc_i^{\#} - Conc_j^{\#})}{Conc_i^{\#}} \times 100 \quad (2)$$

where *Diff* and *Rel* are the absolute and relative concentration difference for the *ETA_#* level when the *i* and *j* scenarios are considered. In the following figures, positive and negative values are presented with different colors, assigning white to zero differences.

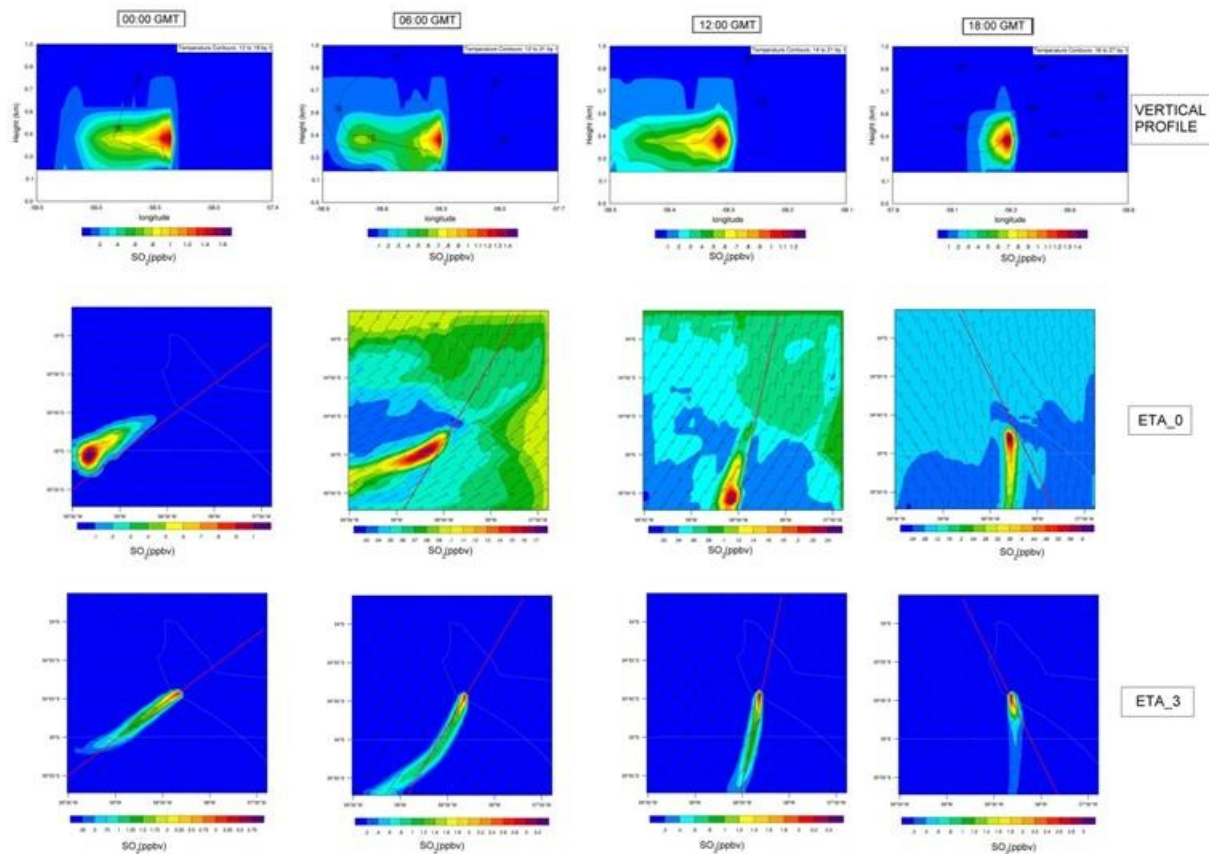


Figure 6: Idem Figure 5 but for the *ALL_3* scenario.

The difference is always performed in the same order, so positive difference values indicates greater absolute concentrations for the first scenario while negative difference indicates greater values for the second scenario. Even though all scenarios have been compared by pairs, only the figures for *ALL_0* – *ALL_3* are shown because the greater changes are observed between these two extreme scenarios.

Figure 7 shows the $Diff_{ALL_0-ALL_3}$ and $Rel_{ALL_0-ALL_3}$ values taken at the *ETA_0* level, and absolute concentrations obtained for the *ALL_0* and *ALL_3* scenarios. In this case we are considering concentration distribution from full emission at surface level compared to full emissions at the highest level. The *Diff* positive values mean that contribution from the first scenario is higher than the one for the second, and the other way around for negative values. In the upper panel negative absolute differences are not clearly visible because of their small magnitude. On the other hand, the relative differences shown in the lower right panel highlights these small

changes, identifying two distinct sections: a northern predominant plume for the *ALL_0* scenario (predominant red), and a southern oriented plume for the *ALL_3* case (predominant blue). This pattern can be explained by the wind fields on *ETA_3* level which are oriented further south than those at the surface.

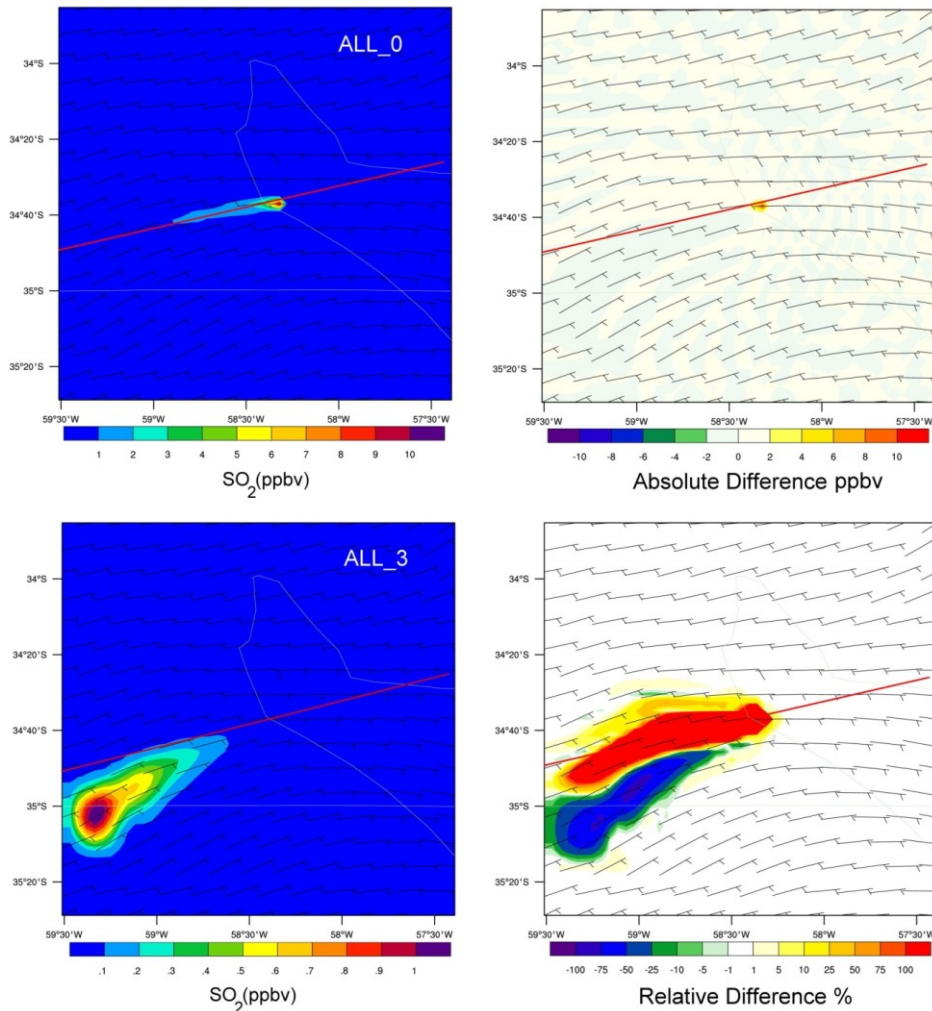


Figure 7: Absolute and relative differences between *ALL_0* and *ALL_3* scenarios for *ETA_0* level. Relative differences can easily surpass 100%. Notice that greater relative differences could appear in places where the absolute differences are not at their maxima.

Figure 8 shows the vertical profile differences associated with Figure 7. Once more, the concentrations in surface and lower levels are greater for the *ALL_0* scenario, while the *ALL_3* emissions generate higher concentrations at higher levels. Yellow/red patterns correspond to lower emissions and blue/green pattern are for emissions in the highest levels. Higher absolute differences in the vertical plane are a consequence of the altitude of the PBL. To conclude, higher emissions are dispersed mainly in the southern direction and distributed in higher levels; and the near surface emissions are oriented further north and towards the lower levels. These figures depict two distinct processes: in the horizontal plane the dispersion is mostly governed by different wind

directions at each level; in the vertical plane the dispersion is controlled by the presence of the PBL.

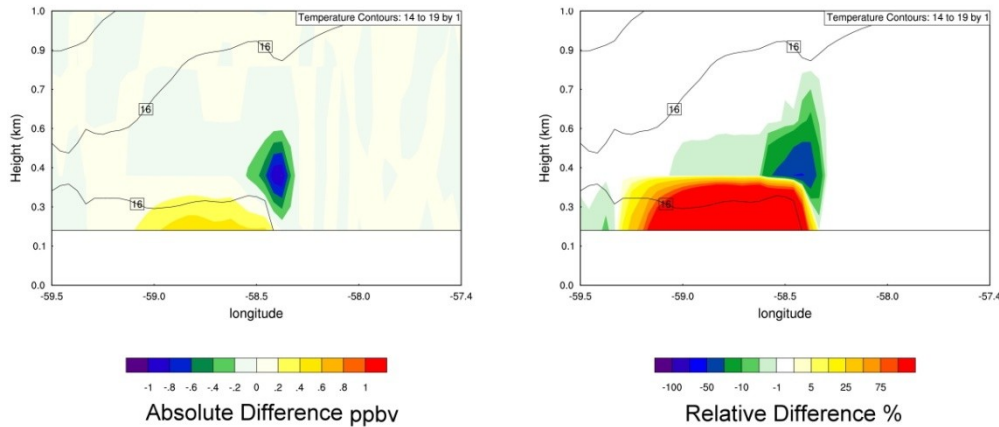


Figure 8: Vertical differences between *ALL_0* (left) and *ALL_3*(right) scenarios. Since the main plume direction is different in each level, the vertical plane selection defines the impact area and the differences obtained. In this case, the maximum concentration for the *ALL_0* case was selected. Notice that an analogous representation could be obtained by selecting the *ALL_3* main direction.

Next, we present a similar analysis as shown in Figure 7 and Figure 8 but for all the *ETA_#* levels (Figure 9). The left panel shows absolute differences while the relative values are presented in the right. For the *ETA_0* and *ETA_1* levels, the absolute differences are positive (yellow to red), while for the *ETA_2* and *ETA_3* levels, the negative values predominate (green to blue). For example, the absolute difference in the *ETA_1* panel shows the contribution coming from the emission at the upper level as a green dot. While, the yellow spot indicates the contribution to this level arising from the near surface emission. The corresponding panel in the relative differences also presents a similar situation to the one explained in Figure 7.

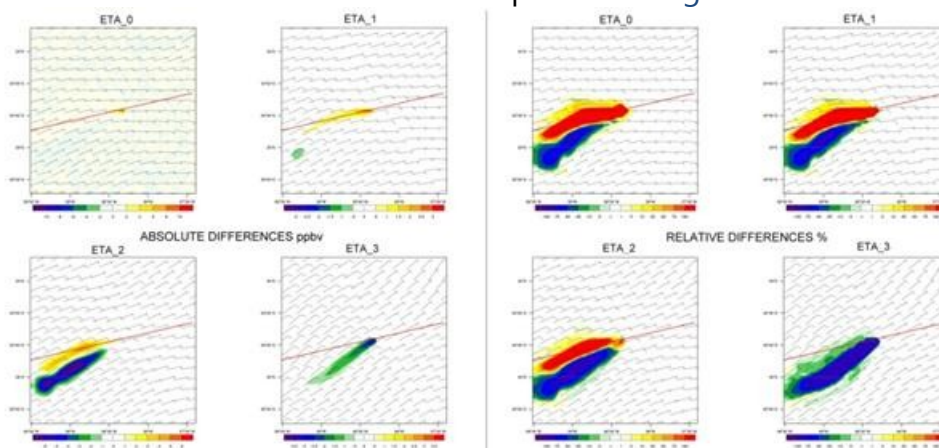


Figure 9: Absolute (left) and relative (right) differences between *ALL_0* and *ALL_3* scenarios for *ETA_0*, *ETA_1*, *ETA_2* and *ETA_3*. Upper left panels (*ETA_0*) are the same as Figure 7.

When the *ETA_3* level is analyzed, negative absolute differences are observed,

indicating that the primary source of pollutants is the self level considered. There are not positive relative differences for this level and the absolute and relative differences appear at the same locations, representing the very weak impact of surface level emissions on ETA_3 concentrations. Because of the meteorological conditions, the dispersion impacts are greater among layers in the downward direction.

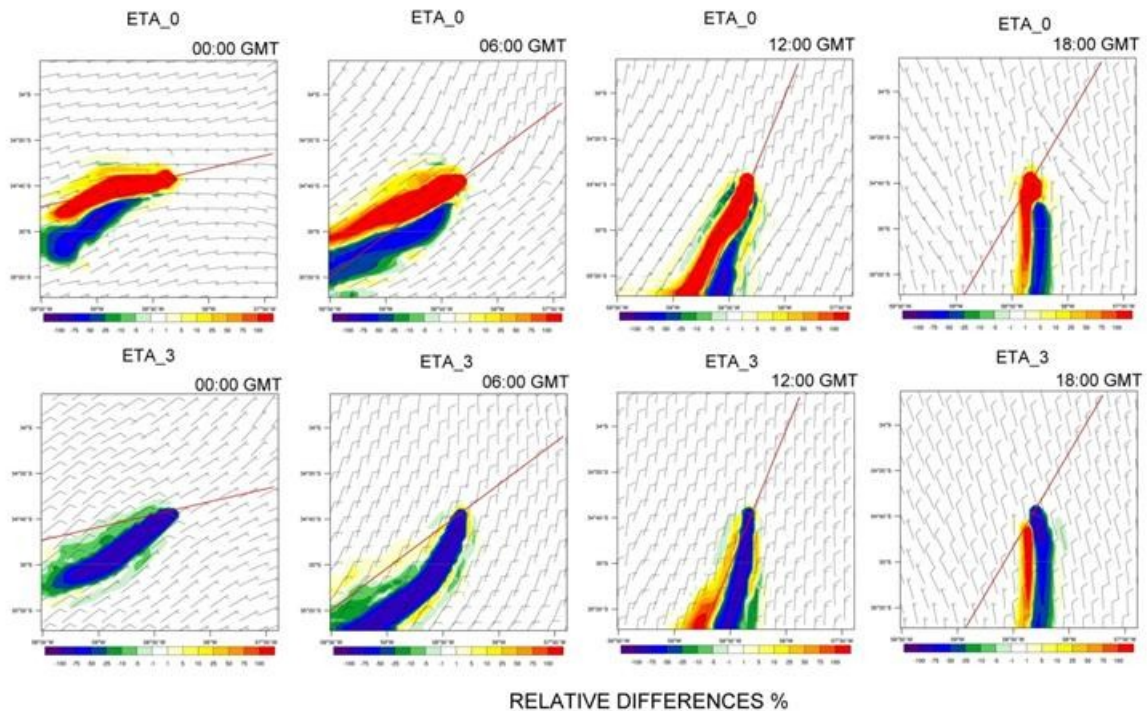


Figure 10: Time dependent relative differences between ALL_0 and ALL_3 scenarios for ETA_0 (top) and ETA_3 (bottom) levels.

Figure 10 shows the temporal evolution of relative differences in pollutant concentrations at ETA_0 and ETA_3 level for the selected set of extreme scenarios. Even though the differences are aligned to the main plume direction, the contribution of the emissions coming from different levels has always the same pattern. This can be explained considering that the wind field for the upper levels is rotating counter-clock wise keeping approximately the same phase between them. Furthermore, after 12:00 GMT the emission from the lowest level has reached the upper layer as a consequence of the ascension of the PBL.

4.5 Statistical Analysis

In order to obtain a quantitative description of the differences over the entire spatial domain at each altitude level, it is necessary to perform a statistical analysis. In this respect, we applied the Willmott (1982) proposed statistical measures. We will take differences between concentrations at two levels at the time combining all emission scenarios for the entire simulation period. For each pair of modeled concentration values, a signed difference ($M1_i - M2_i$) was calculated. The *Mean Bias*

Error (MBE) was computed in order to provide an indication of the main average contributor to the level considered (i.e. if positive, the self layer is dominant; if negative, other layer is dominant). Zero values indicate an equal contribution from both layers with equal spatial distributions. The *Root Mean Square Error* (RMSE) highlights absolute concentrations differences and their spatial patterns. Similar information as the RMSE is given with the *Mean Absolute Error* (MAE), summarizing the mean absolute differences. Willmott's *index of agreement* (d), indicates a correlation between the contribution from the two layers, being the unity (1.0) the value for the maximum agreement.

Figure 11 summarizes the MBE for SO₂ concentration obtained for the stacks emitting at the simulated ETA levels, against the concentration in the other levels. Notice that the error is positive when the difference is calculated between the emitting level and any higher one. On the other hand, the error is negative when the difference is between the emitting level and any other located below this one.

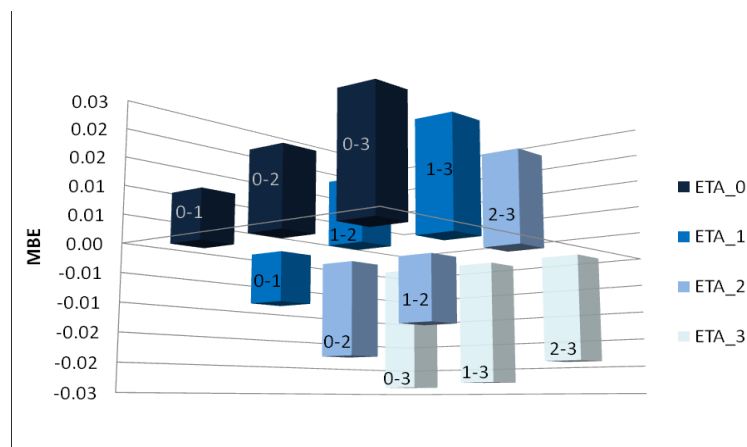


Figure 11: Plots of MBE for the SO₂ simulated concentrations with the stacks emitting in each ETA level against the concentration in the other ones, specified in each box. The color of the box indicates the level

where differences are taken (i.e. dark blue: surface level ETA₀; 0-3 means the emitting scenarios are All₀ and All₃).

Depicting the small variations in the hour-to-hour concentrations, the MBE in the ETA₁ and ETA₂ levels are smaller and their average absolute values are comparable in magnitude. The greatest differences are seen in the ETA₃ level, about 300% (in absolute values) greater than the differences obtained for the other ETA_# cases.

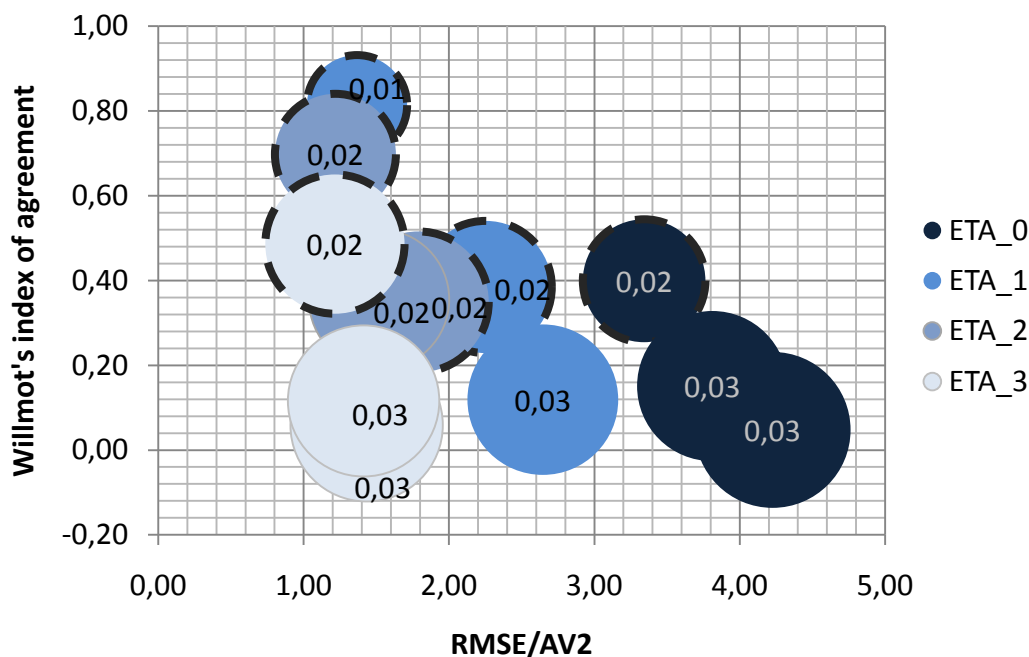


Figure 12: Bubble chart showing the relationship between several performance statistics for each level.

The quantity displayed in the X-axis is a relative difference measure, calculated as the root mean square error divided by the average of the SO_2 concentration (AV2). In the Y-axis scale is represented the Willmott's index of agreement. The area of the plots is proportional to the MAE, indicated in each circle. Dashed lines emphasize the plots showing differences between each level and another one contiguous.

The MBE in the ETA_0 level displays intermediate values. Other evaluation statistics are shown in Figure 12. The coordinates of each circle display in the X axis the RMSE divided by the average SO_2 concentration, the Y axis represent the Willmott's index of agreement. The radius is proportional to the MAE. A perfect agreement would be represented by a point located in the position (0,1) with an small radio.

Clearly, when comparing the differences between contiguous levels, the Willmott's index is higher for each ETA case. That means that SO_2 concentrations are very similar when emission occurs in one level or another neighbor one. This is especially true for concentrations simulated in the intermediate levels. Also, for the emissions in ETA_1 and ETA_2 levels, the relative difference is the lowest in all cases. Note that the MAE for the emissions in the extreme levels are comparable in magnitude and higher than the MAE for the levels in-between them. However, for the ETA_0 case, the relative difference is the higher one, indicating that the surface level is particularly sensitive to changes in emissions in the other levels. A similar analysis can also be done applying the *Kruskal-Wallis* test, a non parametric method for testing equality of populations. Table 3 presents the results of the comparison among concentration distribution in all levels for the $ALL_#$ cases. The numbers indicate the period of time for which contribution of the two emission scenarios agree with a significance level of 0.05. Notice that a good agreement can be seen in the contiguous levels (over the diagonal). The ALL_0 and ALL_3 emission scenarios generate concentration

distributions with higher differences between levels. In this case, 12% of the time the difference between emitting in those levels is significant.

	ALL_1	ALL_2	ALL_3
ALL_0	90%	91%	88%
ALL_1		93%	85%
ALL_2			98%

Table 3: Percentage of the hours simulated in which the distributions compared agree, with the significance level $\alpha = 0.05$ for all $ETA_{\#}$ levels.

Figure 13 compares the relative differences between the scenarios where emissions are spatially allocated in different levels: *AVG*, *MID*, *WANG1*, *WANG2*, *EXT* and *ALL_3*. The scenarios *AVG*, *MID*, *WANG1* and *WANG2* seem all to differ greatly from the *EXT* and *ALL_3*. The vertical disaggregation of the emissions in the scenarios *MID*, *WANG1* and *WANG2* generates similar concentration values in all levels, since the relative difference is very small in all cases (see the radius of the spheres). The *AVG* scenario is a little different from those only at ETA_0 and ETA_3 levels. Consequently, the spatial allocation of the emissions is important when emissions are in the extreme levels, since statistics show that concentration profiles generates the greatest differences when ETA_0 and ETA_3 are involved.

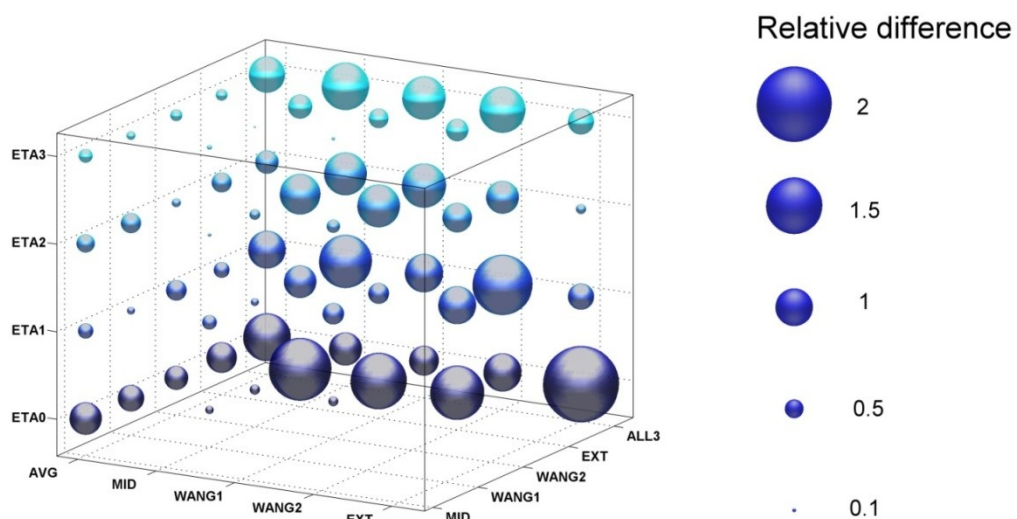


Figure 13: Bubble plot of relative difference, calculated as RMSE divided by the average SO_2 concentration, for all scenarios with vertical distribution of the emissions, for all $ETA_{\#}$ levels.

The Kruskal-Wallis tests for these scenarios are shown in the Table 4.

	MID	WANG1	WANG2	EXT	ALL3
AVG	100%	100%	100%	100%	87%
MID		100%	100%	92%	91%

WANG1			100%	98%	94%
WANG2				96%	89%
EXT					88%

Table 4: Percentage of the hours simulated in which the distributions compared agree, with the significance level $\alpha = 0.05$ for all $ETA_#$ levels. The greatest differences appear when emissions are not distributed in the intermediate levels; i.e. the *EXT* and *ALL3* scenarios.

The scenarios *AVG*, *MID*, *WANG1* and *WANG2* generate in all levels the same concentration distribution for the given significance level. The *EXT* vertical distribution produces similar patterns but not in all the hours simulated. On the other hand, the *ALL_3* scenario differs from the rest of the vertical distributions in many hours of the simulation period.

5 CONCLUSIONS AND FUTURE PLANS

In order to analyze the dependence of primary pollutants concentrations with the altitude of emission, a sensitivity analysis of the WRF/Chem was performed considering different scenarios where the altitude of an industrial stack was modified. The model has the capability to generate wind fields for the different altitude levels considered, and consequently it computes the dispersion of pollutants at each layer accordingly.

The simulation results show small to large sensitivity to height of pollutant emission. The smaller differences are observed when emissions occur predominantly in the middle levels (*ALL_1*, *ALL_2*, *MID*, *WANG1* and *WANG2* cases), so the impact of vertically allocating stack emissions is not critical, unless the altitude of the PBL is surpassed. The Kruskal-Wallis analysis shows that only for the daytime hours, when the PBL height is minimum, the pollutants concentration lead to different distributions. Therefore, the use of more complex pollutant vertical allocation schemes probably will not give a more accurate representation of dispersion in air quality simulations.

However, the largest sensitivity is found when the pollutants are released near surface or at elevated levels. The *ALL_0*, *ALL_3* and *EXT* schemes exhibit high negative and positive bias when comparing concentrations among intermediate levels, as RMSE and MBE values showed. Such differences can be explained by behavior of meteorological variables at different heights. Since the pollutant plume predominant direction depends on the altitude of emissions, there are increasing differences between the postulated scenarios as the relative altitude of emission is increased. Also, the mixing layer depth is a key factor since its diurnal transition defines the volume for dilution of the emitted pollutants and the near-surface concentrations.

For air quality modeling, a crucial factor is the specification of accurate emissions inventories, and a great uncertainty is the role of the vertical allocation of these emissions. Stack heights are parameters not easily available and distribution of the emissions on the vertical are based on few studies, deriving generic vertical profiles. It

was shown that care should be taken, when specifying surface and elevated sources. The correct definition of these stacks will surely benefit on the simulation accuracy. However, no significant differences exist in allocating the emissions in any intermediate level, resulting only in small variations in the concentration patterns.

In the near future, the authors plan to perform real cases computations, including complete emissions inventories for Buenos Aires and other cities, with the aim of characterizing the regional air quality over those regions. More research is needed to evaluate the effects of vertical distribution of the emissions in secondary pollutants. Once the real regions are correctly described, different economic-growing scenarios will be analyzed, considering the estimated increase on transport, residential and industrial emissions. Also, the capability of the model to study trans-boundary pollution problems, both for primary and secondary species, will be analyzed.

6 ACKNOWLEDGEMENTS

The authors would like to thank NCAR (*National Center for Atmospheric Research*), NCEP (*National Centers for Environmental Prediction*) and the associated institutes involved in the development of WRF/Chem model for freely providing the source code and for the help given throughout tutorials and forums. This work was supported by the UTN-FRM, CONICET, and the ANPCyT research project PICT 2005. 23-32686.

REFERENCES

- Allende, D., Cremades, P., Puliafito, E., Perez Gunella, F., Fernandez, R., Estimación de un factor de riesgo de exposición a la contaminación urbana para la población de la Ciudad de Buenos Aires, *Avances en Energías Renovables y Medio Ambiente*, en evaluación, 2010.
- Cruzate, G., L. Gomez, M.J. Pizarro, P. Mercury and S. Bancharo, Mapas de suelos de la República Argentina, *Proyecto PNUD ARG/85/019*. Instituto de Suelos y EEAs del INTA, 2007. <http://geointa.inta.gov.ar>
- Emmons, L., Walters, S., Hess, P., Lamarque, J., Pfister, G., Fillmore, D., Granier, C., Guenther, A., Kinnison, D., Laepple, T., Orlando, J., Tie, X., Tyndall, G., Wiedinmyer, C., Baughcum, S., and Kloster, S., Description and evaluation of the Model for Ozone and Related chemical Tracers, version 4 (MOZART-4). *Geosci. Model Dev.*, 3, 43-67, 2010.
- Grell, G., Peckham, S., Schmitz, R., McKeen, S., Frost, G., Skemerock, W., Eder, B., Fully coupled "online" chemistry within the WRF model. *Atmospheric Environment*, 39, 6957-6975, 2005.
- Meiyun, L., Oki, T., Holloway, T., Streets, D., Bengtsson, M., Kanae, S., Long-range transport of acidifying substances in East Asia--Part I: Model evaluation and sensitivity studies, *Atmospheric Environment*, 42, 5939-5955., 2008.
- Michalakes, J.G., McAtee, M., Wegiel, J., Software Infrastructure for the Weather Research and Forecast Model, in proceedings of UGC 2002, June, Austin, Texas,

- 13pp, 2002. <http://www.mmm.ucar.edu.ar/wrf/users/documents>
- NEI: National Emissions Inventory Data & Documentation, Environmental Protection Agency (EPA), United States, 2005. <http://www.epa.gov/ttn/chief/net/2005inventory.html>
- Peckham, S., Grell, G., McKeen, S., Fast, J., Gustafson, W., Ghan, S., Zaveri, R., Easter, R., Barnard, J., Chapman, E., Wiedeinmyer, C., Schmitz, R., Salzman, M., Freitas, S. WRF/Chem Version 3.2 Users Guide, National Center for Atmospheric Research (NCAR), USA, 2010. http://ruc.noaa.gov/wrf/WG11/Users_guide.pdf
- Placet, M., Mann, C.O., Gilbert, R.O., Niefer, M.J., Emissions of ozone precursors from stationary sources: a critical review. *Atmospheric Environment* 34, 2183e-204, 2000.
- Puliafito, E., Allende, D., Calidad del aire en ciudades intermedias. *Proyecciones*, Año 5, N.2, Publicación de posgrado e investigación de la F.R. Bs. As., UTN, pp. 33-52, 2007.
- Puliafito, E., Quaranta, N., Contaminación Atmosférica en la Argentina: Contribuciones de la II Reunión Anual PROIMCA. Universidad Tecnológica Nacional (UTN). ISBN: 978-950-42-0119-9, 2009.
- RDA: Research Data Archive, Computational and Information Systems Laboratory (CISL) at the National Center for Atmospheric Research (NCAR), 2010. <http://dss.ucar.edu>
- Rodriguez, E., Morris, C.S., Belz, J., Chapin, E., Martin, J., Daffer, W., Hensley, S., An assessment of the SRTM topographic products, Technical Report JPL D-31639, Jet Propulsion Laboratory, Pasadena, California, 143 pp., 2005.
- Schürmann, G., Algieri, A., Hedgecock, I., Manna, G., Pirrone, N., Sprovieri, F., Modelling local and synoptic scale influences on ozone concentrations in a topographically complex region of Southern Italy. *Atmospheric Environment*, 43, 4424-4434., 2009.
- Scire, J.S., Strimaitis, D.G., Yamartino, R.J., A user's guide for the CALPUFF dispersion model (version 5.0). Earth Tech Inc., 2000.
- Seinfeld J.H., Pandis, S.N, Atmospheric Chemistry and Physics: From Air Pollution to Climate Change. Second Ed. Wiley, John & Sons, Incorporated, 2006.
- Stockwell, W. R., Middleton, P., Chang, J. S., and Tang, X., The second generation regional acid deposition model chemical mechanism for regional air quality modeling. *Journal of Geophysical Research*, 95, 16343-16367, 1990.
- US EPA, User's Guide for the Industrial Source Complex (ISC3) Dispersion Models, Office of Air Quality Planning and Standards, 1995.
- Wang, W., Bruyère, C., Duda, M., Dudhia, J., Gill, D., Lin, H-C., Michalakes, J., Rizvi, S., Zhang, X., Advanced Research WRF (ARW) Version 3 Modeling User's Guide, Mesoscale & Microscale Meteorology Division, National Center for Atmospheric Research (NCAR), USA., 2009. http://www.mmm.ucar.edu.ar/wrf/users/docs/arw_v3.pdf
- Wang, X., Liang, X.-Z., Jiang, W., Tao, Z., Wang, J. X.L., Liu, H., Han, Z., Liu, S., Zhang, Y., Grell, G.A., Peckham, S. E., WRF-Chem simulation of East Asian air quality: Sensitivity

to temporal and vertical emissions distributions, *Atmospheric Environment*, 44, 5, 660-669, 2010.

Willmott, C.J., Some comments on the Evaluation of Model Performance. *Bulletin of the American Meteorological Society*, 63, 1309–1313, 1982.

Ying, Z., Xuexi, T., Guohui, L., Sensitivity of ozone concentrations to diurnal variations of surface emissions in Mexico City: A WRF/Chem modeling study. *Atmospheric Environment*, 43, 851-859, 2009.

Zhang, Y., Wen, X.Y., Jang, C., Simulating chemistry-aerosol-cloud-climate feedbacks over the continental U.S. using the online-coupled Weather Research Forecasting Model with chemistry (WRF/Chem). *Atmospheric Environment*, 44, 3568-3582, 2010.